Acta Crystallographica Section D
Biological Crystallography
ISSN 1399-0047

Crystallographic analysis and biochemical applications of a novel penicillin-binding protein/β-lactamase homologue from a metagenomic library

Tri Duc Ngo,[a]‡ Bum Han Ryu,[b]‡ Hansol Ju,[b] Eun Jin Jang,[b] Kyeong Kyu Kim[a]* and T. Doohun Kim[b]*

[a]Department of Molecular Cell Biology, Samsung Biomedical Research Institute, Sungkyunkwan University School of Medicine, Suwon 440-746, Republic of Korea, and [b]Department of Applied Chemistry and Biological Engineering, College of Engineering, Ajou University, Suwon 443-749, Republic of Korea

‡ These authors contributed equally to this work.

Correspondence e-mail: kyeongkyu@skku.edu, doohunkim@ajou.ac.kr

Received 26 March 2014
Accepted 29 June 2014

PDB references: Est-Y29, 4p6b; Est-Y29–4NP, 4p87; Est-Y29–DEP, 4p85

Interest in penicillin-binding proteins and β-lactamases (the PBP-βL family) is increasing owing to their biological and clinical significance. In this study, the crystal structure of Est-Y29, a metagenomic homologue of the PBP-βL family, was determined at 1.7 Å resolution. In addition, complex structures of Est-Y29 with 4-nitrophenyl phosphate (4NP) and with diethyl phosphonate (DEP) at 2.0 Å resolution were also elucidated. Structural analyses showed that Est-Y29 is composed of two domains: a β-lactamase fold and an insertion domain. A deep hydrophobic patch between these domains defines a wide active site, and a nucleophilic serine (Ser58) residue is located in a groove defined primarily by hydrophobic residues between the two domains. In addition, three hydrophobic motifs, which make up the substrate-binding site, allow this enzyme to hydrolyze a wide variety of hydrophobic compounds, including fish and olive oils. Furthermore, cross-linked Est-Y29 aggregates (CLEA-Est-Y29) significantly increase the stability of the enzyme as well as its potential for extensive reuse in various deactivating conditions. The structural features of Est-Y29, together with biochemical and biophysical studies, could provide a molecular basis for understanding the properties and regulatory mechanisms of the PBP-βL family and their potential for use in industrial biocatalysts.

1. Introduction

Bacterial penicillin-binding proteins (PBPs) and β-lactamases (βLs) constitute a large family of serine proteases that perform essential functions in the synthesis and maintenance of cell-wall peptidoglycan (Macheboeuf *et al.*, 2006). PBPs catalyze the final transpeptidation and carboxypeptidation steps in the biosynthesis of peptidoglycan, while βLs provide bacterial protection against β-lactam antibiotics (Sauvage *et al.*, 2008; Majiduddin *et al.*, 2002). These two enzymes are of monophyletic origin (PBP-βL family) and are diversified by local structural changes and domain fusions (Meroueh *et al.*, 2003; Hall & Barlow, 2003; Massova & Mobashery, 1998). Based on phylogenetic analysis, amino-acid sequence, crystal structure and domain organization, bacterial PBP-βLs can be divided into low-mass penicillin-binding proteins (classes A to C), high-mass penicillin-binding proteins (classes A to C) and β-lactamases (classes A to D). The molecular size of PBP-βLs varies from ~20 to 45 kDa, indicating that these proteins have undergone extensive diversification through modification of structural elements.

To date, several bacterial enzymes have been identified to have active-site features similar to those of PBP-βL proteins (PBP-βL homologues). These include an esterase (EstB) from *Burkholderia gladioli* (Wagner *et al.*, 2002), membrane-bound penicillin receptors (BlaR) from *Bacillus licheniformis* and *Staphylococcus aureus* (Kerff *et al.*, 2003; Wilke *et al.*, 2004; Birck *et al.*, 2004), a 6-aminohexanoate dimer hydrolase (Hyb-24) from *Flavobacterium* sp. K172 (Negoro *et al.*, 2005), a group of bacterial glutaminases (Brown *et al.*, 2008; Yoshimune *et al.*, 2006), a simvastatin synthase (LovD) from *Aspergillus terreus* (Gao *et al.*, 2009) and a family VIII carboxylesterase (EstU1; Cha *et al.*, 2013). Furthermore, LACTB, a mammalian mitochondrial PBP-βL homologue found in many metazoan organisms including humans, also shares structural features with class B low-mass penicillin-binding proteins (Peitsaro *et al.*, 2008; Smith *et al.*, 2001). The amino-acid residues for enzymatic activity in bacterial PBP-βL proteins, including the catalytic serine residue, are largely conserved in all metazoan homologues with phylogenetic relationships. Little is known about the structure and function of PBP-βL homologues or LACTB; however, studies have shown that the PBP-βL homologues possesses diverse catalytic functions including β-lactam hydrolysis, DD-peptide hydrolysis and carboxylester hydrolysis. Furthermore, a causative link between LACTB and obesity has been observed, which suggests that LACTB can affect metabolic regulation and mitochondrial organization (Polianskyte *et al.*, 2009; Chen *et al.*, 2008).

Previous studies identified a novel PBP-βL homologue (Est-Y29) by activity screening with a metagenomic library (Yoon *et al.*, 2007). In this study, we elucidated the crystal structure of Est-Y29 at 1.7 Å resolution both alone and in complex with two esterase inhibitors. This could provide a framework for understanding the structure and function of PBP-βL family proteins. Furthermore, the biochemical functions of immobilized enzymes were investigated for possible biotechnological applications.

2. Materials and methods

2.1. Bacterial strains, enzymes and reagents

Cloning and expression of Est-Y29 were performed using *Escherichia coli* XL1-Blue cells (Qiagen, California, USA). Enzyme substrates, antibiotics and LB broth were obtained from Sigma–Aldrich (Seoul, Republic of Korea). PD-10 and Ni–NTA columns were purchased from GE Healthcare Biosciences (Pennsylvania, USA) and all other chemicals used in this study were of reagent grade and were obtained from commercial sources.

2.2. Sequence analysis

To identify related enzymes in the PBP-βL family, the NCBI protein sequence database was searched for sequences similar to the primary sequence of Est-Y29 using *PSI-BLAST* (Jones & Swindells, 2002). All amino-acid sequences were retrieved in FASTA format. Multiple sequence alignments were performed with *Clustal Omega* (Sievers *et al.*, 2011) and results were rendered for analysis using *ESPript* (Gouet *et al.*, 2003).

2.3. Protein purification and crystallization

Protein expression and purification methods have been described previously (Kim *et al.*, 2009). Briefly, XL1-Blue cells were inoculated in 100 ml LB medium containing 100 µg ml^{-1} ampicillin and expression was induced at 310 K for 3 h using 1 m*M* isopropyl β-D-1-thiogalactopyranoside (IPTG). Cells were disrupted by sonication and resuspended in buffer *A* (50 m*M* sodium phosphate pH 8.0, 300 m*M* NaCl, 10 m*M* imidazole). After the solution had been centrifuged at 20 000 rev min^{-1}, the supernatant obtained was applied onto an Ni–NTA column after extensive washing and equilibration with buffer *A*. The protein bound to the column was removed by gradient elution using buffer *A* containing 50–450 m*M* imidazole. The purified protein was then concentrated to 10 mg ml^{-1} in phosphate-buffered saline pH 7.4 using an Amicon Ultrapure-15 centrifugal filter (30 kDa MWCO, Millipore, USA). Purification of selenomethionine-derivatized (SeMet) Est-Y29 was performed in the same way as that for the native protein, except that 1 m*M* DTT (dithiothreitol) was added to all buffers. Crystallization was performed using the microbatch crystallization method at 295 K with commercially available screening kits (Hampton Research, California, USA). Diffraction-quality crystals of native Est-Y29 and SeMet Est-Y29 were obtained after a 1 d incubation at 287 K in 2.0 *M* sodium formate in 0.1 *M* sodium acetate trihydrate buffer pH 4.6. Est-Y29 was mixed with 1 m*M* 4-nitrophenyl phosphate (for Est-Y29–4NP) and diethyl phosphonate (for Est-Y29–DEP) to obtain a final protein concentration of 8 mg ml^{-1} and then incubated for 5 min. Crystals of inhibitor-bound Est-Y29 were obtained using reservoirs consisting of 1 *M* sodium citrate, 100 m*M* sodium acetate pH 4.6.

2.4. Biochemical characterization of Est-Y29

Matrix-assisted laser desorption/ionization time-of-flight mass spectrometry (MALDI-TOF-MS) was performed in positive-ion mode with a Voyager DE STR system (Applied Biosystems, National Collaborative Inter-University Research Facilities, Seoul, Republic of Korea). Dynamic light-scattering (DLS) profiles were measured with a Zetasizer Nano S system (Malvern Instruments Ltd, Malvern, England). Est-Y29 preparations were passed through a 0.1 µm filter before dilution and were allowed to equilibrate to 293 K prior to DLS measurements. Multiple data-set replicates were analyzed using the *DTS* 5.10 software supplied by the manufacturer, and the calculated hydrodynamic radius was corrected to standard solvent conditions.

The hydrolase activity of Est-Y29 was determined by measuring the absorbance at 405 nm using a VersaMax or Bio-Rad 680 microplate reader (Kim *et al.*, 2012; Hwang *et al.*, 2010). The naphthyl-group derivatives 1-naphthyl acetate (1-NA), 2-naphthyl acetate (2-NA), 1-naphthyl butyrate (1-NB) and 1-naphthyl phosphate (1-NP) were used as substrates. The standard assay solution consisted of 0.9 ml

Table 1
Data-collection and refinement statistics for native and SeMet Est-Y29 structures.

Values in parentheses are for the outermost resolution shell.

	Native Est-Y29	SeMet Est-Y29		
		Peak	Inflection	Remote
Data collection				
Space group	*I*4	*I*4		
Unit-cell parameters				
$a = b$ (Å)	121.54	121.87		
c (Å)	155.17	154.40		
$\alpha = \beta = \gamma$ (°)	90	90		
Molecules in asymmetric unit	2	2		
Wavelength (Å)	1.00000	0.97888	0.97917	0.96395
Resolution (Å)	50.0–1.70	30–1.79	30–1.79	30–1.79
$R_{\rm merge}$ (%)†	8.3 (29.8)	7.7 (16.2)	6.7 (16.7)	5.3 (16.8)
Mean $I/\sigma(I)$	45.0 (9.1)	25.5 (12.6)	25.2 (11.1)	24.8 (9.8)
Completeness (%)	99.5 (100)	99.5 (99.9)	99.6 (100)	99.6 (100)
Multiplicity	7.2 (7.2)	7.6 (7.4)	7.6 (7.4)	7.6 (7.4)
Refinement				
Resolution (Å)	30–1.70			
No. of reflections	115954			
$R_{\rm work}$‡/$R_{\rm free}$§ (%)	17.04/18.79			
No. of atoms				
Protein	5938			
Ligand/ion	—			
Water	898			
B factors, all atoms (Å^2)				
Main chain	16.6			
Side chain	17.4			
R.m.s.d.¶				
Bond lengths (Å)	0.01			
Bond angles (°)	1.25			

† $R_{\rm merge} = \sum_{hkl}\sum_i |I_i(hkl) - \langle I(hkl)\rangle| / \sum_{hkl}\sum_i I_i(hkl)$, where $I_i(hkl)$ is the single intensity of reflection *hkl* as determined by the *i*th measurement and $\langle I(hkl)\rangle$ is the mean intensity of reflection *hkl*. ‡ $R_{\rm cryst} = \sum_{hkl} ||F_{\rm obs}| - |F_{\rm calc}|| / \sum_{hkl} |F_{\rm obs}|$, where $F_{\rm obs}$ is the structure-factor amplitude of the observed structure and $F_{\rm calc}$ is the structure-factor amplitude calculated from the model. § $R_{\rm free}$ is calculated in the same manner as $R_{\rm cryst}$ using 5% of all reflections excluded from the refinement stages using high-resolution data. ¶ Root-mean-square deviation.

Table 2
Data-collection and refinement of the complex structures of native Est-Y29 with inhibitors.

Values in parentheses are for the outermost resolution shell.

	Est-Y29–4NP	Est-Y29–DEP
Data collection		
Space group	*I*4	*I*4
Unit-cell parameters		
$a = b$ (Å)	121.73	122.08
c (Å)	155.830	155.290
$\alpha = \beta = \gamma$ (°)	90	90
Molecules in asymmetric unit	2	2
Wavelength (Å)	1.00000	1.00000
Resolution (Å)	33–2.0	50.0–2.0
$R_{\rm merge}$† (%)	7.9 (30.3)	8.8 (31.7)
Mean $I/\sigma(I)$	28.15 (6.27)	30 (6.03)
Completeness (%)	99.8 (99.7)	100 (100)
Multiplicity	7.3 (7.4)	7.5 (7.6)
Refinement		
Resolution (Å)	30–2.0	29–2.0
No. of reflections	72376	67804
$R_{\rm work}$‡/$R_{\rm free}$§ (%)	17.77/21.22	19.31/22.74
No. of atoms		
Protein	6009	6010
Ligand/ion	28	16
Water	816	754
B factors (Å^2)		
Main chain	16.17	16.35
Side chain	17.15	18.10
R.m.s.d.¶		
Bond lengths (Å)	0.011	0.011
Bond angles (°)	1.247	1.254

† $R_{\rm merge} = \sum_{hkl}\sum_i |I_i(hkl) - \langle I(hkl)\rangle| / \sum_{hkl}\sum_i I_i(hkl)$, where $I_i(hkl)$ is the single intensity of reflection *hkl* as determined by the *i*th measurement and $\langle I(hkl)\rangle$ is the mean intensity of reflection *hkl*. ‡ $R_{\rm cryst} = \sum_{hkl} ||F_{\rm obs}| - |F_{\rm calc}|| / \sum_{hkl} |F_{\rm obs}|$, where $F_{\rm obs}$ is the structure-factor amplitude of the observed structure and $F_{\rm calc}$ is the structure-factor amplitude calculated from the model. § $R_{\rm free}$ is calculated in the same manner as $R_{\rm cryst}$ using 5% of all reflections excluded from the refinement stages using high-resolution data. ¶ Root-mean-square deviation.

0.3 m*M* substrate solution in 20 m*M* Tris–HCl pH 8.0 with 30 µg Est-Y29 protein. Reaction mixtures were incubated for 5 min and the absorbance was determined at 310 nm. For enantioselectivity analysis, Est-Y29 was reacted with either (*R*)- or (*S*)-solution. The (*R*)- and (*S*)-solutions consisted of phenol red (2 g l^{-1}), 20 m*M* Tris–HCl pH 8.0 and 300 m*M* (*R*)- or (*S*)-methyl-3-hydroxy-2-methylpropionate. For the hydrolysis of tertiary alcohol esters (TAEs), 100 µg Est-Y29 was added to substrate-mixture solutions containing phenol red (2 mg ml^{-1}) and either 25 m*M* *t*-butyl acetate, linalyl acetate or α-terpinyl acetate in 20 m*M* Tris–HCl pH 8.0 buffer.

2.5. X-ray data collection

Native and SeMet crystals were equilibrated in cryosolvent containing 6 *M* sodium formate before being flash-cooled in a cold nitrogen stream. Est-Y29–4NP and Est-Y29–DFP crystals were transferred to cryosolvent consisting of 1 *M* sodium citrate, 100 m*M* sodium acetate pH 4.6, 25% glycerol. X-ray diffraction data were collected at 100 K using an ADSC Quantum 210 detector on beamline NW12 at the Photon Factory (PF), Japan and an ADSC Quantum 315 CCD on beamline 4A at the Pohang Accelerator Laboratory (PAL), Republic of Korea. The data were indexed, integrated and scaled using *HKL*-2000 (Otwinowski & Minor, 1997). Data-collection and processing statistics for Est-Y29 are summarized in Tables 1 and 2.

2.6. Structure determination and refinement

The structure was determined from the SeMet data using the multiwavelength anomalous diffraction (MAD) method. *SOLVE* (Terwilliger & Berendzen, 1999) and *RESOLVE* (Terwilliger, 2001) were used to identify and refine the selenium sites. Phases were calculated and used to produce a 2.0 Å resolution electron-density map. *RESOLVE* was used for electron-density modification. Automated model building was performed by *ARP*/*wARP* (Langer *et al.*, 2008) and the model was refined against the SeMet data using *REFMAC* (Murshudov *et al.*, 2011). The refined SeMet model was then used as a template for molecular replacement of the native data set using *MOLREP* (Vagin & Teplyakov, 2010). The model was refined through many steps using *REFMAC* and *PHENIX* (Adams *et al.*, 2010) and the quality of the final model was evaluated with *PROCHECK* (Laskowski *et al.*, 1993). No residues fell within the disallowed region of the Ramachandran plot. The structures of Est-Y29–4NP and

Est-Y29–DEP were determined by molecular replacement using the native structure of Est-Y29 as a molecular template. The three-dimensional structures were analyzed using *PyMOL* (Schrödinger) for graphical presentation.

2.7. Cross-linked enzyme aggregate (CLEA) preparation

To prepare the CLEAs, purified Est-Y29 (500 µg) was precipitated with 80% ammonium sulfate in 25 m*M* Tris–HCl pH 8.0. Glutaraldehyde (final concentration 0.1 m*M*) was then added to cross-link the aggregates, followed by incubation for 12 h at room temperature with gentle agitation (Kim *et al.*, 2012; Taboada-Puig *et al.*, 2011). The suspension was centrifuged at 15 000*g* and 277 K for 10 min and the pellet containing the CLEAs was resuspended and washed repeatedly until enzyme activity could no longer be detected in the supernatant. The resulting CLEAs were resuspended and stored at 277 K for further use. The activities of free Est-Y29 and CLEA-Est-Y29 were determined by monitoring the hydrolysis of *p*-nitrophenyl acetate (C_2). The surface morphology of CLEA-Est-Y29 was examined using SUPRA 55VP (Carl Zeiss, New York, USA). Images were taken at an accelerating voltage of 2 kV at various magnifications ranging from 10 000× to 200 000×. For the reusability study, CLEA-Est-Y29 was used in an additional nine cycles. After each cycle, the pellet was resuspended and washed repeatedly (usually three times) until enzyme activity could no longer be detected in the supernatant. For chemical stability analysis, the effects of several chemical compounds on the enzymatic activities of CLEA-Est-Y29 and free Est-Y29 were determined. The enzymatic activity in the buffer-only condition was defined as 100%. Stabilities were determined by measuring the residual activity of the enzyme after 1 h of incubation at 298 K. All experiments were repeated at least three times.

3. Results and discussion

3.1. Sequence analyses and conserved motifs of Est-Y29

The primary sequence of Est-Y29 consists of a single 392-amino-acid polypeptide chain. Close matches to Est-Y29 in an NCBI search were mainly annotated as putative penicillin-binding proteins or class C β-lactamases. Sequence analysis was performed to clarify the relationship of Est-Y29 to other PBP-βL family proteins. As shown in Fig. 1(*a*), Est-Y29 was clustered in a branch between class B low-molecular-weight penicillin-binding proteins (PBPs) and class C β-lactamases. Therefore, Est-Y29 shared limited sequence identity with penicillin-binding proteins from *Streptomyces* sp. R61 (15.2%, UniProt P15555), *Bacillus subtilis* (14.5%, UniProt P32959) and *Ochrobactrum anthropi* (11.4%, UniProt Q9ZBA9) and with β-lactamases from *Escherichia coli* K-12 (16.3%, UniProt P00811), *O. anthropi* (12.8%, UniProt Q9F3Z2) and *Enterobacter cloacae* (12.6%, UniProt P05364). Furthermore, Est-Y29 showed low sequence homology with the LACTB family. Furthermore, ∼90 residues are conserved between Est-Y29 and human LACTB (15.5% sequence identity).

PBP-βL family proteins contain three typical motifs (motifs I, II and III) that are proposed to be involved in substrate recognition and catalysis (Fig. 1*a*). These motifs are highly conserved, with relatively similar spacing along the polypeptide chains, which is evidence of a common evolutionary origin (Peitsaro *et al.*, 2008; Macheboeuf *et al.*, 2006). Motif I includes a catalytic serine residue in the invariant tetrapeptide S*xx*K, which is catalytically fundamental to the enzyme's acylation and deacylation steps. In this motif, Ser acts as a nucleophile, while Lys is involved in the stabilization of the oxyanion. In the case of Est-Y29, a nucleophilic Ser58 is also found in the characteristic tetrapeptide,

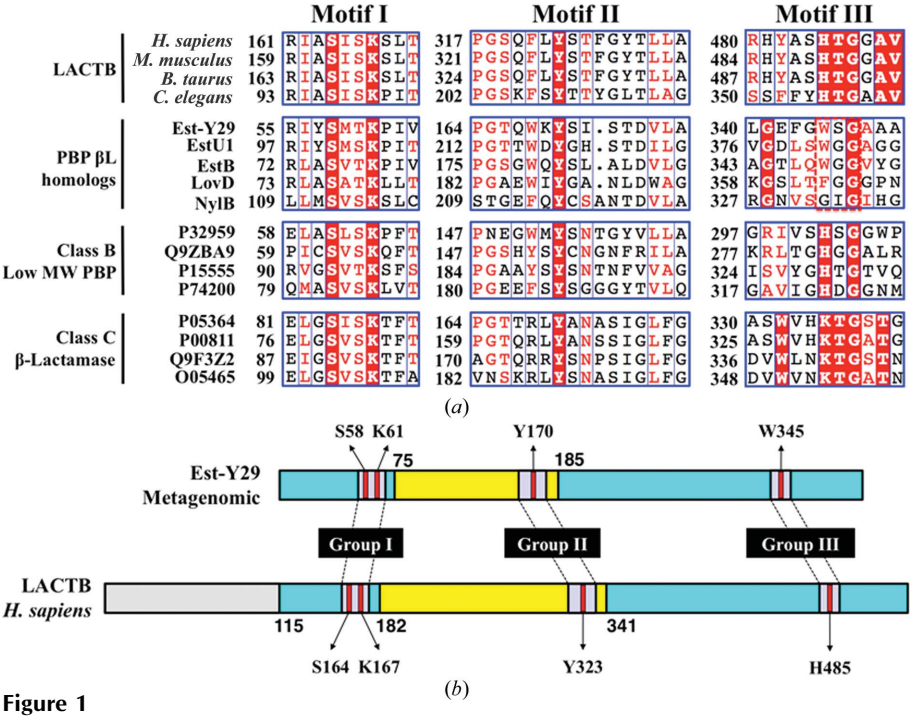

Figure 1
Multiple sequence alignment and overall structural organization of Est-Y29. (*a*) Multiple sequence alignment of Est-Y29 and related proteins was performed using *Clustal Omega* 1.2 and *ESPript* 2.2. All sequences were retrieved from the NCBI protein-sequence database. Amino-acid sequences of the PBP-βL family and PBP-βL-like family were aligned with that of Est-Y29; only three motifs (motifs I, II and III) are shown for clarity. Highly conserved residues are shown in red. Note that the catalytic residues of motifs I and II are highly conserved compared with those of motif III. (*b*) The structural organization of Est-Y29 and human mitochondrial β-lactamase (*Homo sapiens* LACTB) is shown for comparison. Note that the structural organization of Est-Y29 is quite similar to that of *H. sapiens* LACTB, except for the putative transit peptides at the N-terminus. The relative positions of motifs I, II and III are shown with the catalytic residues of Est-Y29 (Ser58, Lys61, Try170 and Trp345).

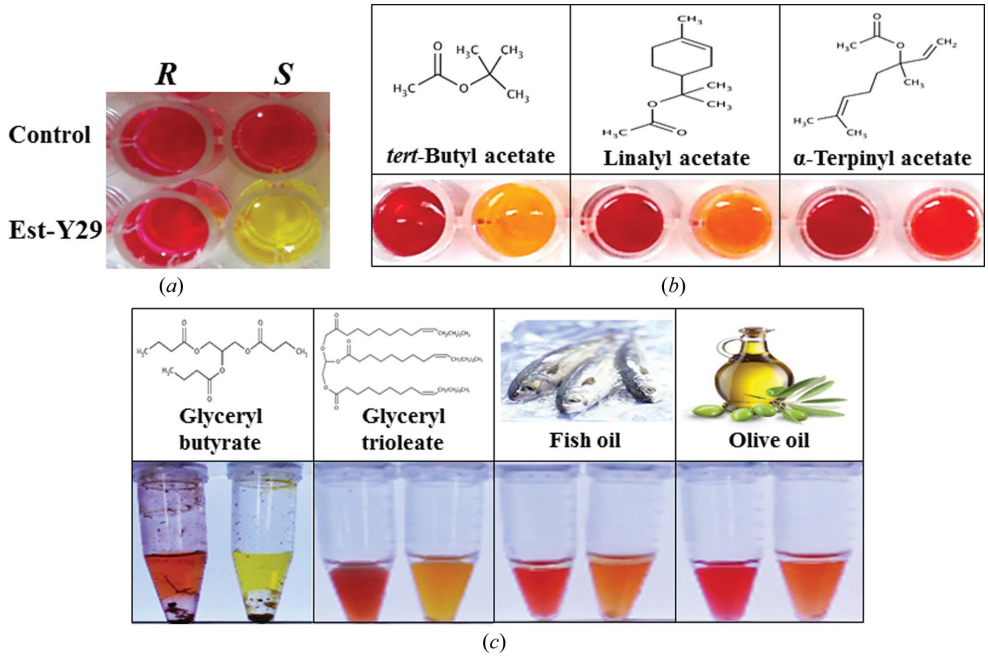

Figure 2
pH-shift assay of Est-Y29. (*a*) Enantioselectivity analysis was conducted with (*R*)- and (*S*)-methyl-3-hydroxy-2-methylpropionate. The appearance of a yellow colour indicates hydrolysis of the (*S*)-substrate by Est-Y29. (*b*, *c*) Hydrolysis of tertiary alcohol esters, glyceryl esters and oils. The results of enzyme hydrolysis with chemical structures are shown. The first and second columns in each box included buffer alone and Est-Y29, respectively. (*b*) Hydrolysis of tertiary alcohol esters (TAEs) by Est-Y29 was measured. (*c*) Hydrolysis of glyceryl esters (glyceryl tributyrate and glyceryl trioleate) and oils (fish oil and olive oil) was measured.

Ser58-*x*-*x*-Lys61. Another conserved residue among these proteins is a tyrosine (Tyr170 in Est-Y29) in motif II. The hydroxyl group of the tyrosine in this motif is believed to be responsible for deacylation, similar to the serine of the S*x*N motif of other classes in the PBP-βL family (Sauvage *et al.*, 2008; Silvaggi *et al.*, 2003). Interestingly, unlike other conserved motifs, motif III is not completely conserved in the PBP-βL family or its homologue proteins. In the case of metazoan LACTB family proteins, His-Thr-Gly is found in the centre of motif III. However, in class B low-molecular weight PBPs only the histidine is conserved among these three residues, while Lys is found in the same position in the class C βL proteins (Peitsaro *et al.*, 2008; Zapun *et al.*, 2008). Distinct from other members of PBP-βL family proteins, in Est-Y29 Trp354 is replaced instead of the His or Lys residues (Fig. 1*a*). The same phenomenon is also observed in EstB from *B. gladioli*, in which the Trp residue is followed by a Gly residue in the downstream amino-acid sequence (Petersen *et al.*, 2001). Interestingly, the indole group of Trp exerts various functions such as charge relay, substrate binding and oxyanion-hole stabilization (Richter *et al.*, 2010; Lee *et al.*, 2009; Baurin *et al.*, 2009). For example, Trp154 in the OXA-10 β-lactamase from *Pseudomonas aeruginosa* has been suggested to play a role in the activity and stability of the enzyme (Baurin *et al.*, 2009). In addition, analysis of the known crystal structures revealed that the backbone carbonyl of this glycine makes up the hydrogen-bonding network in the oxyanion hole.

The LACTB family is composed of mammalian proteins that share sequence similarity to PBP-βLs proteins. Specifically, three such groups (I, II and III) have been identified through sequence comparisons with PBP-βL family proteins (Peitsaro *et al.*, 2008; Smith *et al.*, 2001). Human LACTB protein has an N-terminal domain with about 100 amino acids and no sequence similarity to any other bacterial PBP-βL proteins (Fig. 1*b*). Sequence comparison shows that the three groups and their catalytic residues are conserved, suggesting that the PBP-βL family of proteins, its homologues and LACTB all share common features in their secondary and tertiary structures.

3.2. Biochemical characterization of Est-Y29

Initial biochemical analysis of Est-Y29 was conducted using MALDI-TOF mass spectrometry and dynamic light scattering (DLS). Mass-spectrometric analysis showed a major peak (m/z) at 42.6 kDa corresponding to the calculated molecular weight of Est-Y29 (Supplementary Fig. S1*a*[1]). The hydrodynamic profile of Est-Y29 based on DLS indicated a uniform shape (Supplementary Fig. S1*b*). The substrate specificity of Est-Y29 for naphthyl-derivative ester substrates was analyzed in 25 m*M* Tris–HCl buffer pH 7.5 at 293 K. As shown in Supplementary Fig. S1(*c*), the highest activity was obtained with 2-naphthyl acetate (2-NA), followed by 1-naphthyl acetate (1-NA) and 1-naphthyl butyrate (1-NB). However, Est-Y29 could not hydrolyze 1-naphthyl phosphate (1-NP). For enantioselectivity analysis, a pH-drop colourimetric assay

[1] Supporting information has been deposited in the IUCr electronic archive (Reference: CB5058).

was used with (*R*)- and (*S*)-methyl-3-hydroxy-2-methylpropionate (Hwang *et al.*, 2010). Hydrolysis of the ester compounds was monitored for colour and absorbance changes resulting from a drop in pH. Following incubation with Est-Y29, only the reaction mixture containing the (*S*)-enantiomer turned yellow, clearly indicating the (*S*)-specific enantioselectivity of Est-Y29 (Fig. 2*a*). Almost no hydrolytic activity was observed in the reaction mixture containing the (*R*)-enantiomer.

The ability of Est-Y29 to hydrolyze tertiary alcohol esters (TAEs) was examined using *tert*-butyl acetate, linalyl acetate and α-terpinyl acetate as substrates (Ngo *et al.*, 2013). As shown in Fig. 2(*b*), Est-Y29 hydrolyzed *tert*-butyl acetate, linalyl acetate and the bulky α-terpinyl acetate. Because tertiary alcohols are valuable building blocks for pharmaceuticals, Est-Y29 is a promising biocatalyst for pharmaceutical applications (Kourist & Bornscheuer, 2011). The ability of Est-Y29 to hydrolyze several lipids was further investigated in Eppendorf tubes containing lipid emulsions and a phenol red indicator, which signalled the release of fatty acids by a red-to-yellow colour change. As expected, the glyceryl tributyrate emulsion became yellow almost instantly after the addition of Est-Y29. A significant level of hydrolytic activity toward glyceryl trioleate, fish oil and olive oil was also detectable (Fig. 2*c*). Therefore, Est-Y29 efficiently hydrolyzed fish oil and olive oil in addition to glyceryl tributyrate and glyceryl trioleate. Considering that eicosapentaenoic acid (EPA) and docosahexaenoic acid (DHA) are normally obtained from fish oil or olive oil, Est-Y29 is a good candidate for the industrial-scale production of oils enriched in EPA and DHA (Pérez *et al.*, 2011; Chakraborty & Paulraj, 2008).

3.3. Molecular architecture of Est-Y29

The crystal structure of Est-Y29 was determined at 1.7 Å resolution with an R_{work} of 17.04% (R_{free} = 18.79%) using the multiple-wavelength anomalous dispersion (MAD) method (Table 1). In the native Est-Y29 structure the average *B* factors of the main-chain and side-chain atoms were 16.6 and 17.4 Å^2, respectively. The residues located in positions 224–229 were not visible in the electron density and are therefore missing from the final model. In addition, the inhibitor-bound structures Est-Y29–4NP and Est-Y29–DFP were also determined using molecular replacement at 2.0 Å resolution with reasonable R_{work}/R_{free} values (Table 2).

The overall structure of Est-Y29 is composed of two domains: a β-lactamase fold and a small insertion domain (Fig. 3*a*). The β-lactamase fold has a seven-stranded antiparallel β-sheet (β2, β1, β9, β8, β7, β6 and β5) with four helices on one face (α2, α7, α8, and α9) and two helices on the other (α1 and α10). The small insertion domain includes four α-helices (α3, α4, α5, and α6) and two small antiparallel β-strands (β3 and β4). Together, these two domains create a long, deep hydrophobic active site that is composed of three motifs (motifs I–III). The four residues (Ser58-Met59-Thr60-Lys61) in motif I are found at the N-terminal end of helix α2 (Fig. 3*a*). The loop connecting helix α5 and helix α6 harbours the tyrosine (Tyr170) of motif II. The tryptophan (Trp348) and glycine (Gly350) of motif III are situated at the C-terminal end

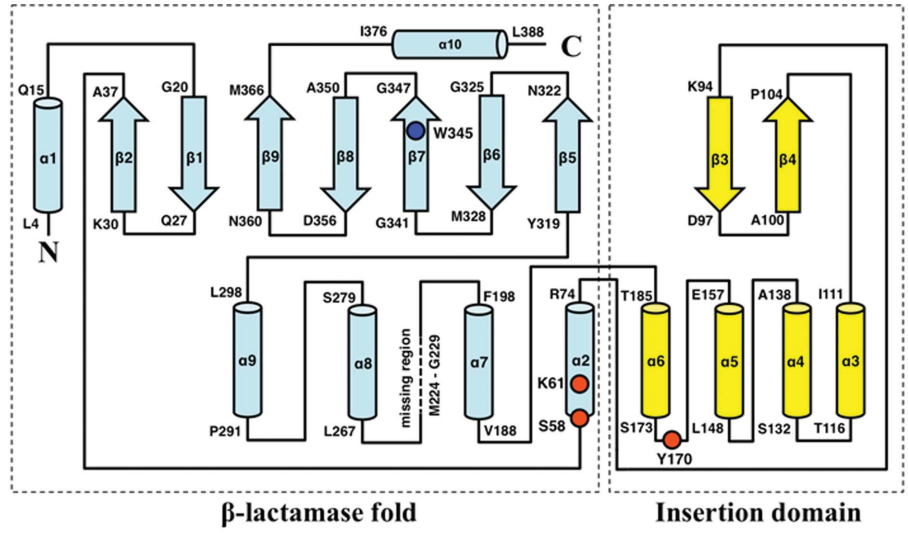

(*a*)

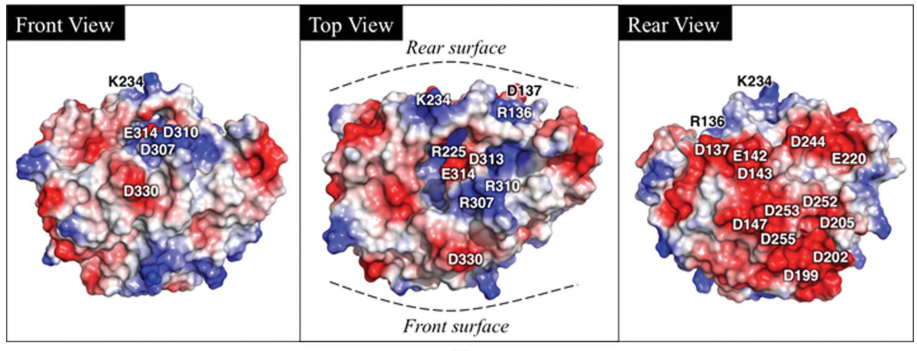

(*b*)

Figure 3
Topology diagram and electrostatic potential of Est-Y29. (*a*) Cyan and yellow regions indicate the domain I (β-lactamase fold) and domain II (insertion domain) regions of Est-Y29, respectively. Secondary structures (ribbon diagram) with catalytic triad residues (red circles) and Trp345 are shown. Regions related to enzyme/substrate binding are marked with distinct labels (blocks A–D, β7 and the β7–β8 turn; see also Fig. 7). (*b*) Surface potential representations of Est-Y29. The substrate-binding pockets of Est-Y29 are shown at the centre of the molecule (left). Two other views corresponding to the lower and upper sides of the substrate-binding pocket (centre and right) are also shown. The molecular surfaces are coloured according to electrostatic potential; positive surface potential is represented in blue and negative surface potential in red. Charged residues in blocks A, B and C (see also Fig. 6*a*) are labelled. It is noteworthy that the rear surface of Est-Y29 consists almost entirely of negatively charged residues.

of β7. Fig. 3(*b*) shows the electrostatic surface of Est-Y29, highlighting the overall positive charge present on one side of the molecule. The large, negatively charged surface is owing to the presence of many aspartic acid and glutamic acid residues, which had not previously been observed in other PBP-βL family proteins.

Est-Y29 showed structural similarity to DD-carboxypeptidase (UniProt P15555; PDB entry 3pte; Kelly & Kuzin, 1995) from *Streptomyces* R61, with an root-mean-square deviation (r.m.s.d.) of 1.86 Å for 288 C^{α} atoms. Est-Y29 also showed structural similarity to a P99 β-lactamase (UniProt P05364; PDB entry 1xx2; J. R. Knox & T. Sun, unpublished work) from *E. cloacae*, with an r.m.s.d. of 2.12 Å for 300 C^{α} atoms. These two enzymes have 15.2 and 12.6% sequence identity to Est-Y29, respectively, and only 23 residues are completely conserved among all three enzymes. Although all of these proteins are composed of a β-lactamase fold and an insertion domain, a structural comparison showed striking differences in the orientations of these domains (Figs. 4*a*–4*c*). In addition, the secondary structure and topology of each

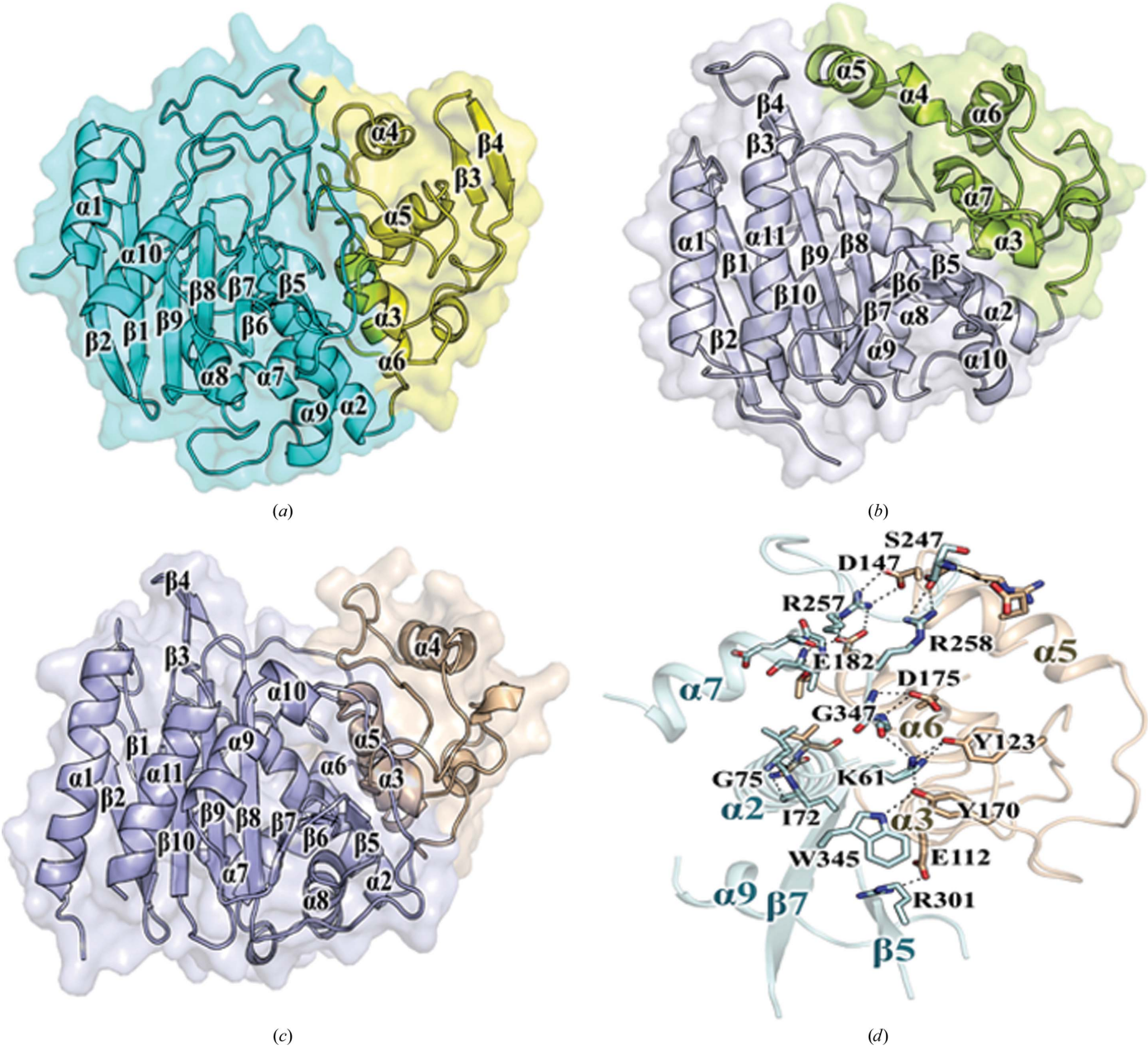

Figure 4
Structural visualization of (*a*) Est-Y29, (*b*) a class B low-molecular-weight PBP (PDB entry 3pte; D-alanyl-D-alanine transpeptidase from *Streptomyces* sp. R61) and (*c*) a class C P99 β-lactamase (PDB entry 1xx2; β-lactamase from *E. cloacae*). The overall structures (ribbon diagram) with enzyme surfaces are shown and domains I and II of each enzyme are distinguished by different colours. Note that the domain orientations in these three enzymes are distinctly different. (*d*) Structural analysis of the domain–domain interface of Est-Y29. Electrostatic interactions and hydrogen bonds are shown with dashed lines.

domain also showed intriguing structural variations among these three proteins. Specifically, an additional β-strand (β5) which was not found in Est-Y29 was present in the central β-sheet of the β-lactamase fold in DD-carboxypeptidase and class C β-lactamase. Furthermore, a large loop (Phe189–Leu267) connecting α7 and α8 was observed in Est-Y29, whereas two short antiparallel strands (β3 and β4) were present in the corresponding region of DD-carboxypeptidase and class C β-lactamase (Silvaggi *et al.*, 2003).

Based on the presence of three conserved α-helices (α3, α4 and α6) in the insertion domain of Est-Y29, which are structurally equivalent to α3, α6 and α7 of DD-carboxypeptidase and α3, α4 and α5 of class C β-lactamase, it is hypothesized that the insertion domains of these enzymes are evolutionally related. However, notable differences among the insertion domains have also been observed. Specifically, two additional short β-strands (β3 and β4) are present between α2 and α3 only in Est-Y29. In DD-carboxypeptidase, two additional short helices (α4 and α5) are located between α3 and α6, while a long helix (α5) was observed in Est-Y29 (Kelly & Kuzin, 1995).

The area of the inter-domain interface in Est-Y29 (1788 Å^2) is similar to those of DD-carboxypeptidase (1780 Å^2) and NylB (1717 Å^2; Negoro *et al.*, 2005) but is larger than those of P99 β-lactamase (1472 Å^2) and LovD (1387 Å^2; Gao *et al.*, 2009). The domain–domain interface was formed mainly by α2, the α4/α5 loop, α6, the α7/α8 loop, α8 and the α9/β5 loop, and includes salt bridges from Arg257 (on the loop between α7 and α8) to Asp147 (on the loop between α4 and α5) and from Arg301 (on the loop between α9 and β5) to Glu112 (on the helix α3). Extensive hydrogen-bonding networks were also formed involving Asp175, Ser247, Arg258, Trp345 and Gly347 of the β-lactamase fold and Lys61, Ile72, Gly75, Tyr123, Tyr170, Asp175 and Glu182 of the insertion domain (Fig. 4*d*).

3.4. Active site of Est-Y29

In the three-dimensional structure of Est-Y29, three conserved motifs are in close proximity at the catalytic centre between a β-lactamase fold and an insertion domain. In a previous study, site-directed mutagenesis of Ser58 to Ala in Est-Y29 resulted in a drastic reduction in the enzyme activity to undetectable levels, confirming that Ser58 acts as a nucleophile in catalysis (Yoon *et al.*, 2007). This serine-containing motif S*xx*K is located at a structurally equivalent position in other members of the PBP-βL family. The active site of Est-Y29 shows a dense hydrogen-bonding network around the catalytic residues. Lys61 N$^{\zeta}$ plays a pivotal role in this network, forming hydrogen bonds to Ser58 O$^{\gamma}$ (2.8 Å), Tyr170 O$^{\eta}$ (3.3 Å), Tyr123 O$^{\eta}$ (2.7 Å) and the carbonyl group of Gly260 (3.0 Å). The carbonyl group of Lys61 is also involved in a hydrogen-bonding network with the amide groups of Val61 (3.4 Å) and Ser65 (2.7 Å) and with Ser65 O$^{\gamma}$ (2.8 Å). In addition, Ser58 O$^{\gamma}$ was found to be spatially separated from Tyr170 O$^{\eta}$ by 2.8 Å and from the carbonyl group of Gly260 by 3.4 Å. Furthermore, the spatial locations of the residues of Est-Y29 (Ser68/Lys71/Tyr170) are similar to those of DD-peptidase (Ser90/Lys93/Tyr190) and class C β-lactamase (Ser81/Lys84/Tyr170), suggesting that Est-Y29 has conformational features characteristic of the PBP-βL family (Fig. 5*a*). To investigate their roles, we replaced Lys61 and Tyr170 with Ala by site-directed mutagenesis, purified the mutant enzymes to homogeneity and assayed the enzymatic

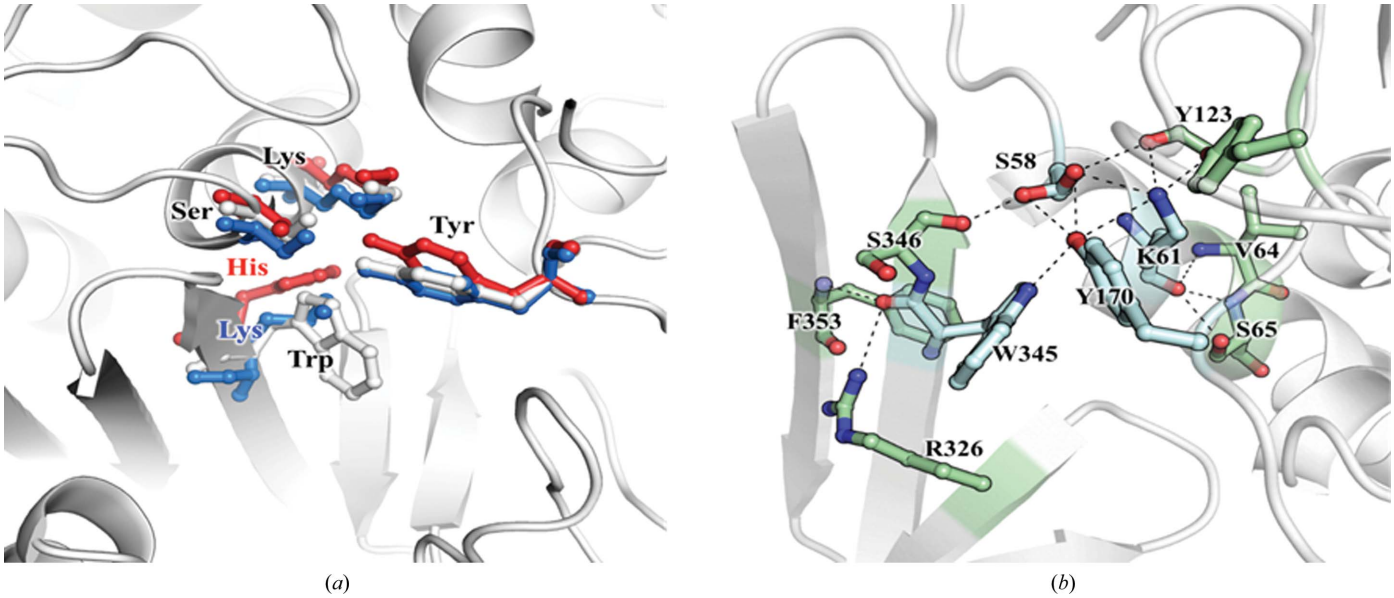

(*a*) (*b*)

Figure 5
Active-site analysis of Est-Y29. (*a*) Structural alignment of the catalytic residues of Est-Y29 (white), DD-carboxypeptidase (cyan) and P99 β-lactamase (light blue). Notably, the Trp in Est-Y29 is replaced by His in DD-carboxypeptidase and Lys in P99 β-lactamase, although all three residues are structurally well aligned in these three enzymes. (*b*) The hydrogen-bonding network of Est-Y29 around the active site is shown. The hydrogen-bond distances are 2.8 Å between Ser58 O$^{\gamma}$ and Tyr170 O$^{\eta}$ and 3.3 Å between Ser58 O$^{\gamma}$ and Lys61 N$^{\zeta}$.

activities using standard assay conditions. A single substitution (Lys61 to Ala or Tyr170 to Ala) resulted in a drastic decrease in hydrolytic activity (Supplementary Table S1), suggesting essential roles for Lys61 and Tyr170 in catalysis. Therefore, Lys61 and Tyr170 are necessary for efficient catalytic activity by participating in the acylation of Ser58 (Sauvage *et al.*, 2008; Macheboeuf *et al.*, 2006). In addition, the position of Trp345 in Est-Y29 was structurally analogous to His329 in DD-peptidase and His335 in class C β-lactamase. Furthermore, the spatial locations of the glycine residues in motif III of Est-Y29 (Gly347), which are involved in oxyanion-hole formation, are similar to those of DD-peptidase (Gly331) and class C β-lactamase (Gly337). A hydrogen bond is formed between Trp345 $N^{\varepsilon1}$ and Tyr170 O^{η} (3.0 Å). In addition, the carbonyl groups of Trp345 are located 3.3 and 3.0 Å from Arg326 $N^{\eta1}$ and the amino group of Phe353, respectively (Fig. 5*b*).

3.5. Substrate-binding cleft of Est-Y29

Although the active sites of the PBP-βL family are structurally related, notable differences are observed in the size and shape of the loops encircling the active sites, the conformational flexibilities of which may be involved in binding substrates and regulating enzyme activity. Although the catalytic sites in the family members are very similar, there are significant positional differences in the regions peripheral to the active sites of Est-Y29, DD-carboxypeptidase and P99 β-lactamase. Specifically, the three regions named the A block (His117–Asp147), B block (Asp199–Thr266) and C block (Ala299–Gly318) of Est-Y29 constitute the majority of the substrate-binding sites (Figs. 6*a* and 6*b*).

The A block is six and 15 residues longer in Est-Y29 than it is in DD-carboxypeptidase and P99 β-lactamase, respectively. This region contains a long extended loop that partially covers

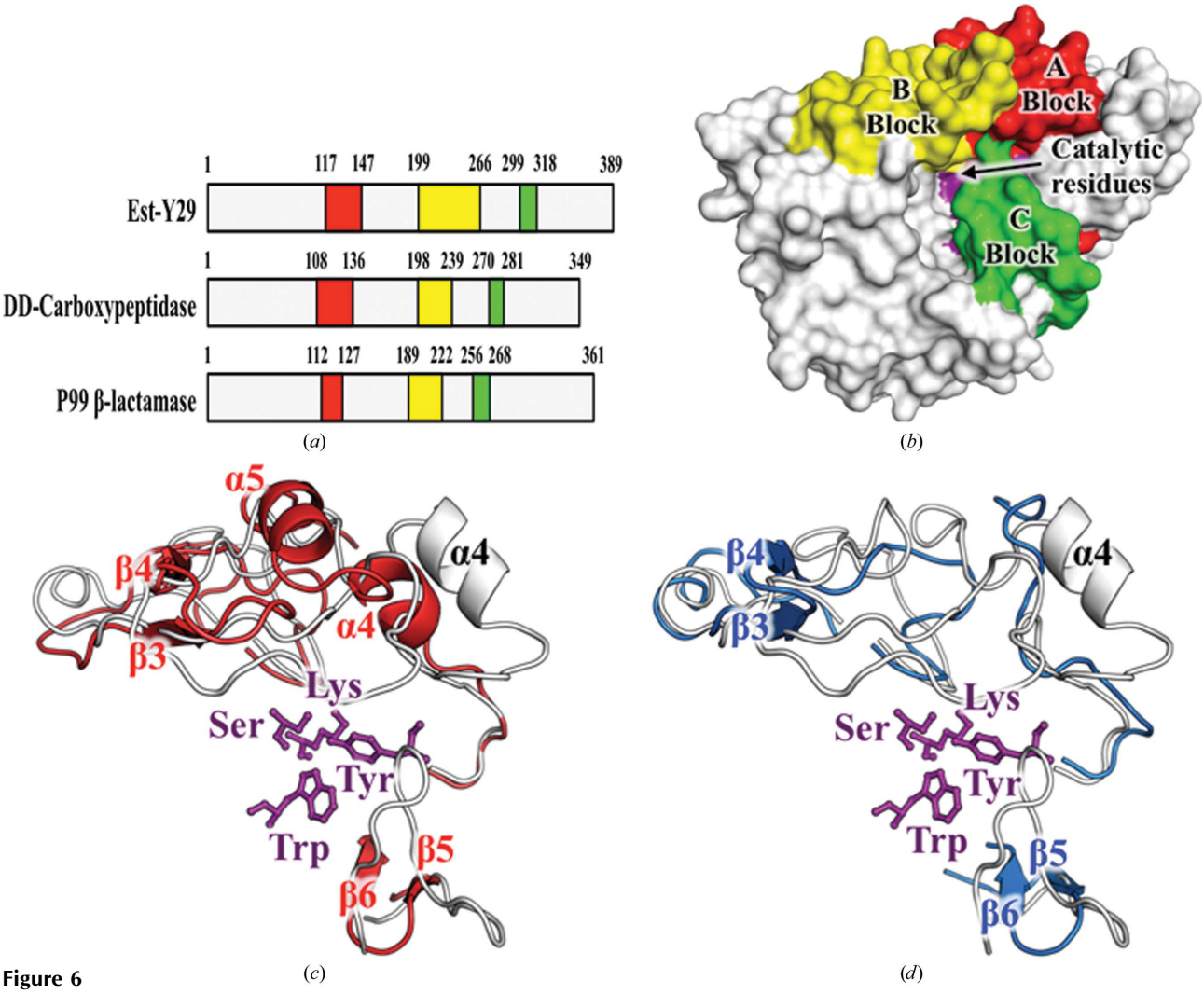

Figure 6
Analysis of the substrate-binding regions. (*a*) Key components of the substrate-binding pockets of Est-Y29, DD-carboxypeptidase and P99 β-lactamase are shown by coloured blocks (A block, His117–Asp147; B block, Asp199–Thr266; C block, Ala299–Gly318). (*b*) Structural analysis of the three blocks in Est-Y29. The A, B and C blocks of Est-Y29 (white), DD-carboxypeptidase (red) and P99 β-lactamase (blue) are shown as ribbon diagrams for structural comparison. The catalytic residues of Est-Y29 are shown as a ball-and-stick representation in purple. It is interesting to note that (*c*) DD-carboxypeptidase and (*d*) P99 β-lactamase have additional rigid β-strands (β3 and β4 in the B block and β5 and β6 in the C block), while Est-Y29 has long flexible loops in these regions.

the active site and forms part of the substrate-binding site. The A block (residues His117–Asp147) of the insertion domain in Est-Y29 forms a protrusion distant from the β-lactamase domain, which is proposed to act as a wide flexible entrance for efficient ligand binding.

Specifically, this block includes two aromatic residues, Tyr123 and Phe125, that are situated on a flexible loop between α3 and α4 with their side chains exposed to the solvent and are implicated in π–π stacking and/or π–cation interactions with the bound ligands. These two residues display high conformational flexibility, suggesting that they play a dynamic role in the opening and closing of the pathway to the active site. In addition, α4 in Est-Y29 is displaced 19 Å from the active site, while two rigid helices in DD-carboxypeptidase and a small irregular loop in P99 β-lactamase limit the size of the active-site pathways in these proteins (Figs. 6*c* and 6*d*). The B block region (Asp199–Thr266), flanked by α7 and α8 in Est-Y29, was 16 and 24 residues longer than the corresponding regions in DD-carboxypeptidase and P99 β-lactamase, respectively. This region, despite its length, makes few contacts with the rest of the protein, which may explain the flexibility that is necessary in the course of catalysis. Although this region forms a main entrance site for the substrate in Est-Y29, access to the corresponding regions of DD-carboxypeptidase and P99 β-lactamase are restricted by two short antiparallel β-strands (β3 and β4; Figs. 6*c* and 6*d*). It is highly likely that the B block of Est-Y29 is significantly more mobile than those of DD-carboxypeptidase and P99 β-lactamase, which is likely to contribute to transient enlargement of the substrate-binding gorge during catalysis. Furthermore, the *B* factors for this region of Est-Y29 were 23.8 Å^2 (main chain) and 23.2 Å^2 (side chains), which are larger than the average *B* factors of the main-chain atoms (16.6 Å^2) and side-chain atoms (17.4 Å^2). Furthermore, the C block (Ala298–Gly318) between α9 and β5, which faces the B block across the active-site cleft, is much longer in Est-Y29 than the corresponding regions in DD-carboxypeptidase and P99 β-lactamase. Access to this region in DD-carboxypeptidase or P99 β-lactamase is also restricted by two antiparallel β-strands (β5 and β6), although the corresponding region of Est-Y29 is composed only of flexible loop regions (Figs. 6*c* and 6*d*).

In contrast to DD-carboxypeptidase and P99 β-lactamase, Est-Y29 has a large binding pocket which may be used to stabilize large hydrophobic substrates. These structural features of the substrate-binding region lead to structural plasticity of Est-Y29, which is consistent with the ability of Est-Y29 to bind and hydrolyze the widest spectrum of substrates among these three enzymes.

3.6. Ligand-bound structures of Est-Y29

Electron-density maps for the 4NP-soaked and DEP-soaked crystals showed clear densities for the nitrophenyl phosphate and covalently bound diethyl phosphonate moieties. Interestingly, the electron-density map of the Met224–Gly229 region of the B block, which forms one side of the catalytic cleft, was poorly defined in the native state but was clearly observed in the inhibitor-bound structures. Specifically, Arg225 and Leu227 were shown to clearly form the substrate-binding cleft for the recognition of the substrates, which suggests that these residues are flexible in the native state but are stabilized by inhibitor binding. The oxyanion was stabilized by the main-chain atoms of Ser58 and Ala348, which are spatially located 2.9 and 3.0 Å from the

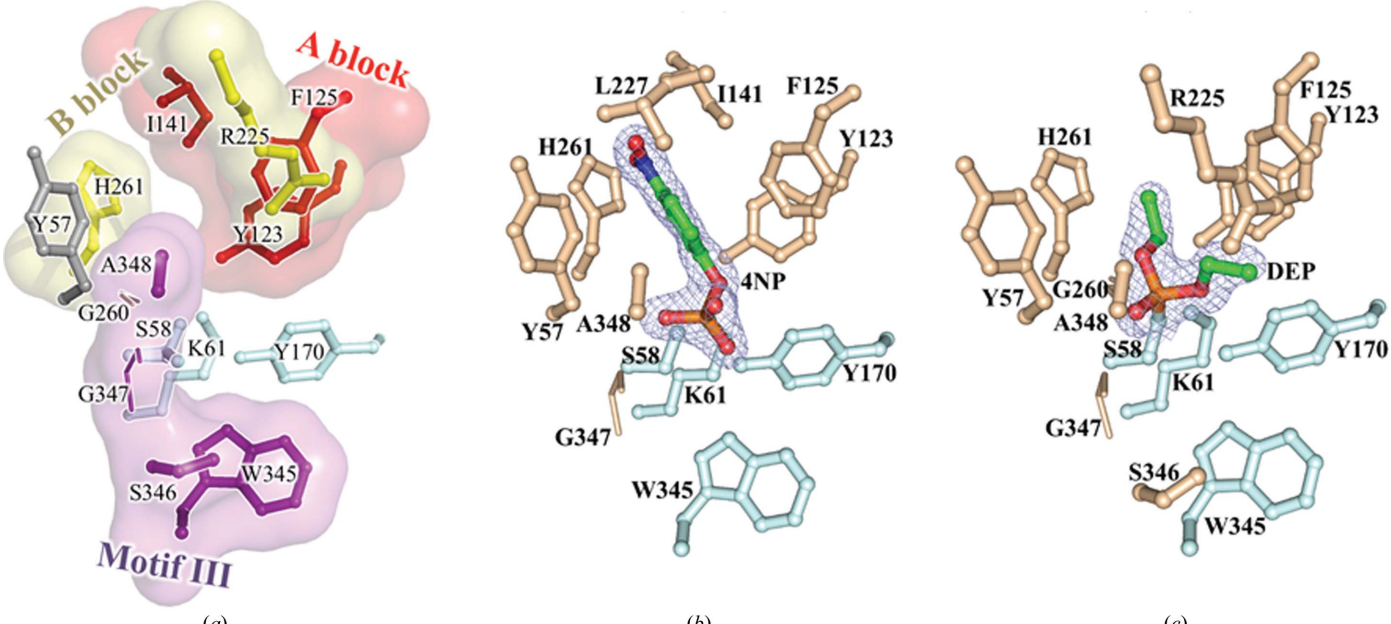

(*a*) (*b*) (*c*)

Figure 7
Ball-and-stick models of Est-Y29 around the active site are shown for (*a*) native Est-Y29, (*b*) *p*-nitrophenyl phosphate (4NP)-bound Est-Y29 and (*c*) diethyl phosphonate (DEP)-bound Est-Y29. In (*a*), residues in the A block (red), the B block (yellow) and and motif III (purple) are also shown with their surfaces. Catalytic triad residues are shown in light cyan.

phosphate group. 4NP and DEP were surrounded by the aromatic rings of Tyr57, Tyr123, Phe125, Tyr170, His261 and Trp345, indicating that these two molecules are mostly trapped within the hydrophobic patch between the domains (Fig. 7). Additional hydrogen bonds and van der Waals interactions were observed with Arg22, Ser58, Tyr170 and the peptide planes of Gly260, Gly347 and Ala348. Furthermore, in the DEP-bound structure the phosphonate group was covalently bound to Ser58 O^{γ}, mimicking the tetrahedral intermediate formed during the hydrolysis of substrates. The distance between Tyr170 O^{η} and Lys61 N^{ζ} was much shorter in the DEP-bound state (2.6 Å) than in the native structure (3.3 Å). Furthermore, a water molecule was 2.8 Å from the hydroxyl group of Tyr170 and may play a role in the protonation of this residue.

3.7. Cross-linked enzyme aggregates (CLEAs) of Est-Y29

Immobilized enzymes are highly specific and efficient catalysts for the preparation of pharmaceutical compounds (Hanefeld *et al.*, 2009). Recently, several enzymes were immobilized as cross-linked aggregates (CLEAs) in order to serve as stable biocatalysts (Ju *et al.*, 2013; Taboada-Puig *et al.*, 2011). In a previous report, Est-Y29 was shown to be significantly effective for the preparation of (*S*)-ketoprofen with high thermostability (Yoon *et al.*, 2007). Furthermore, Est-Y29 efficiently hydrolyzed fish oil and olive oil in addition to glyceryl tributyrate and glyceryl trioleate (Fig. 3*b*). The high stability, the wide variety of substrates and the strict enantioselectivity of Est-Y29 further prompted us to investigate the immobilization of Est-Y29 because immobilized enzymes serve as highly efficient and specific biocatalysts for a wide variety of industrial applications. To investigate the enzyme performance of immobilized Est-Y29, CLEA-Est-Y29 was prepared by precipitating the enzyme with ammonium sulfate followed by glutaraldehyde cross-linking. Scanning electron-microscopic images of CLEA-Est-Y29 showed large globular structures with a high surface density (Supplementary Figs. S2*a* and S2*b*). CLEA-Est-Y29 was able to be reused for 18 assay cycles without significant activity loss (Supplementary Fig. S2*c*), indicating a degree of stability that is essential for repetitive use as an industrial biocatalyst. The effects of various chemical compounds on the activities of CLEA-Est-Y29 and free Est-Y29 were examined by measuring the residual activity after a 1 h incubation. The enzymatic activities of CLEA-Est-Y29 in the presence of 30% ethanol and 5 m*M* PMSF underscored the beneficial effect of enzyme immobilization. Specifically, in the presence of 30% ethanol free Est-Y29 lost half of its initial activity within 1 h, while CLEA-Est-Y29 retained 85% of its initial activity during the same time frame (Supplementary Fig. S2*d*). Furthermore, although incubation with 5 m*M* PMSF almost completely inactivated free Est-Y29, the residual activity of CLEA-Est-Y29 remained very similar to the original activity before incubation. Therefore, CLEA-Est-Y29 seems to be effective as a biocatalyst under various nonphysiological conditions.

4. Conclusion

In this study, the crystal structure of Est-Y29, a metagenomic homologue of the PBP-βL family, was determined at 1.7 Å resolution. In addition, complex structures of Est-Y29 with 4-nitrophenyl phosphate (4NP) and diethyl phosphonate (DEP) were also elucidated at 2.0 Å resolution. Crystallographic analyses showed that three enlarged blocks (A, B and C) with extended conformations allow this enzyme to hydrolyze a wide variety of substrates, highlighting the structural plasticity of the substrate-binding regions. Immobilization of Est-Y29 significantly increased the stability of the enzyme in various deactivating conditions, suggesting industrial potential as a biocatalyst in various applications. The structural features of Est-Y29, together with the results of biochemical and biophysical studies, provide a molecular basis for understanding the properties and regulatory mechanisms of the PBP-βL family, as well as a platform for industrial biotechnological applications.

This work was supported by National Research Foundation of Korea grants funded by the Korean Government (NRF-2012S1A2A1A01028907, NRF-2013K2A1A2053659 and NRF-2012R1A1A2000910) to TDK. In addition, KK was supported by the Next-Generation BioGreen 21 Program (SSAC PJ008107), the Korea Healthcare Technology R&D Project (A092006) and a National Research Foundation of Korea (NRF) grant (2011-0028878).

References

Adams, P. D. *et al.* (2010). *Acta Cryst.* D**66**, 213–221.
Baurin, S., Vercheval, L., Bouillenne, F., Falzone, C., Brans, A., Jacquamet, L., Ferrer, J.-L., Sauvage, E., Dehareng, D., Frère, J.-M., Charlier, P., Galleni, M. & Kerff, F. (2009). *Biochemistry*, **48**, 11252–11263.
Birck, C., Cha, J. Y., Cross, J., Schulze-Briese, C., Meroueh, S. O., Schlegel, H. B., Mobashery, S. & Samama, J.-P. (2004). *J. Am. Chem. Soc.* **126**, 13945–13947.
Brown, G., Singer, A., Proudfoot, M., Skarina, T., Kim, Y., Chang, C., Dementieva, I., Kuznetsova, E., Gonzalez, C. F., Joachimiak, A., Savchenko, A. & Yakunin, A. F. (2008). *Biochemistry*, **47**, 5724–5735.
Cha, S.-S., An, Y. J., Jeong, C. S., Kim, M.-K., Jeon, J. H., Lee, C.-M., Lee, H. S., Kang, S. G. & Lee, J.-H. (2013). *Proteins*, **81**, 2045–2051.
Chakraborty, K. & Paulraj, R. (2008). *J. Agric. Food Chem.* **56**, 1428–1433.
Chen, Y. *et al.* (2008). *Nature (London)*, **452**, 429–435.
Gao, X., Xie, X., Pashkov, I., Sawaya, M. R., Laidman, J., Zhang, W., Cacho, R., Yeates, T. O. & Tang, Y. (2009). *Chem. Biol.* **16**, 1064–1074.
Gouet, P., Robert, X. & Courcelle, E. (2003). *Nucleic Acids Res.* **31**, 3320–3323.
Hall, B. G. & Barlow, M. (2003). *J. Mol. Evol.* **57**, 255–260.
Hanefeld, U., Gardossi, L. & Magner, E. (2009). *Chem. Soc. Rev.* **38**, 453–468.
Hwang, H., Kim, S., Yoon, S., Ryu, Y., Lee, S. Y. & Kim, T. D. (2010). *Int. J. Biol. Macromol.* **46**, 145–152.
Jones, D. T. & Swindells, M. B. (2002). *Trends Biochem. Sci.* **27**, 161–164.
Ju, H., Jang, E., Ryu, B. H. & Kim, T. D. (2013). *Bioresour. Technol.* **128**, 81–86.
Kelly, J. A. & Kuzin, A. P. (1995). *J. Mol. Biol.* **254**, 223–236.

Kerff, F., Charlier, P., Colombo, M.-L., Sauvage, E., Brans, A., Frère, J.-M., Joris, B. & Fonzé, E. (2003). *Biochemistry*, **42**, 12835–12843.
Kim, S., Bae, S. Y., Kim, S. J., Ngo, T. D., Kim, K. K. & Kim, T. D. (2012). *Int. J. Biol. Macromol.* **50**, 103–111.
Kim, S., Joo, S., Yoon, S., Kim, S., Moon, J., Ryu, Y., Kim, K. K. & Kim, T. D. (2009). *Acta Cryst.* F**65**, 310–312.
Kourist, R. & Bornscheuer, U. T. (2011). *Appl. Microbiol. Biotechnol.* **91**, 505–517.
Langer, G., Cohen, S. X., Lamzin, V. S. & Perrakis, A. (2008). *Nature Protoc.* **3**, 1171–1179.
Laskowski, R. A., MacArthur, M. W., Moss, D. S. & Thornton, J. M. (1993). *J. Appl. Cryst.* **26**, 283–291.
Lee, L.-C., Chou, Y.-L., Chen, H.-H., Lee, Y.-L. & Shaw, J.-F. (2009). *Biochim. Biophys. Acta*, **1794**, 1467–1473.
Macheboeuf, P., Contreras-Martel, C., Job, V., Dideberg, O. & Dessen, A. (2006). *FEMS Microbiol. Rev.* **30**, 673–691.
Majiduddin, F. K., Materon, I. C. & Palzkill, T. G. (2002). *Int. J. Med. Microbiol.* **292**, 127–137.
Massova, I. & Mobashery, S. (1998). *Antimicrob. Agents Chemother.* **42**, 1–17.
Meroueh, S. O., Minasov, G., Lee, W., Shoichet, B. K. & Mobashery, S. (2003). *J. Am. Chem. Soc.* **125**, 9612–9618.
Murshudov, G. N., Skubák, P., Lebedev, A. A., Pannu, N. S., Steiner, R. A., Nicholls, R. A., Winn, M. D., Long, F. & Vagin, A. A. (2011). *Acta Cryst.* D**67**, 355–367.
Negoro, S., Ohki, T., Shibata, N., Mizuno, N., Wakitani, Y., Tsurukame, J., Matsumoto, K., Kawamoto, I., Takeo, M. & Higuchi, Y. (2005). *J. Biol. Chem.* **280**, 39644–39652.
Ngo, T. D., Ryu, B. H., Ju, H., Jang, E., Park, K., Kim, K. K. & Kim, D. T. (2013). *Acta Cryst.* D**69**, 1726–1737.
Otwinowski, Z. & Minor, W. (1997). *Methods Enzymol.* **276**, 307–326.
Peitsaro, N., Polianskyte, Z., Tuimala, J., Pörn-Ares, I., Liobikas, J., Speer, O., Lindholm, D., Thompson, J. & Eriksson, O. (2008). *BMC Evol. Biol.* **8**, 26.
Pérez, D., Martín, S., Fernández-Lorente, G., Filice, M., Guisán, J. M., Ventosa, A., García, M. T. & Mellado, E. (2011). *PLoS One*, **6**, e23325.
Petersen, E. I., Valinger, G., Sölkner, B., Stubenrauch, G. & Schwab, H. (2001). *J. Biotechnol.* **89**, 11–25.
Polianskyte, Z., Peitsaro, N., Dapkunas, A., Liobikas, J., Soliymani, R., Lalowski, M., Speer, O., Seitsonen, J., Butcher, S., Cereghetti, G. M., Linder, M. D., Merckel, M., Thompson, J. & Eriksson, O. (2009). *Proc. Natl Acad. Sci. USA*, **106**, 18960–18965.
Richter, N., Breicha, K., Hummel, W. & Niefind, K. (2010). *J. Mol. Biol.* **404**, 353–362.
Sauvage, E., Kerff, F., Terrak, M., Ayala, J. A. & Charlier, P. (2008). *FEMS Microbiol. Rev.* **32**, 234–258.
Sievers, F., Wilm, A., Dineen, D., Gibson, T. J., Karplus, K., Li, W., Lopez, R., McWilliam, H., Remmert, M., Söding, J., Thompson, J. D. & Higgins, D. G. (2011). *Mol. Syst. Biol.* **7**, 539.
Silvaggi, N. R., Anderson, J. W., Brinsmade, S. R., Pratt, R. F. & Kelly, J. A. (2003). *Biochemistry*, **42**, 1199–1208.
Smith, T. S., Southan, C., Ellington, K., Campbell, D., Tew, D. G. & Debouck, C. (2001). *Genomics*, **78**, 12–14.
Taboada-Puig, R., Junghanns, C., Demarche, P., Moreira, M. T., Feijoo, G., Lema, J. M. & Agathos, S. N. (2011). *Bioresour. Technol.* **102**, 6593–6599.
Terwilliger, T. C. (2001). *Acta Cryst.* D**57**, 1763–1775.
Terwilliger, T. C. & Berendzen, J. (1999). *Acta Cryst.* D**55**, 1872–1877.
Vagin, A. & Teplyakov, A. (2010). *Acta Cryst.* D**66**, 22–25.
Wagner, U. G., Petersen, E. I., Schwab, H. & Kratky, C. (2002). *Protein Sci.* **11**, 467–478.
Wilke, M. S., Hills, T. L., Zhang, H.-Z., Chambers, H. F. & Strynadka, N. C. J. (2004). *J. Biol. Chem.* **279**, 47278–47287.
Yoon, S., Kim, S., Ryu, Y. & Kim, T. D. (2007). *Int. J. Biol. Macromol.* **41**, 1–7.
Yoshimune, K., Shirakihara, Y., Shiratori, A., Wakayama, M., Chantawannakul, P. & Moriguchi, M. (2006). *Biochem. Biophys. Res. Commun.* **346**, 1118–1124.
Zapun, A., Contreras-Martel, C. & Vernet, T. (2008). *FEMS Microbiol. Rev.* **32**, 361–385.